REVISTAMATÉRIA

V.29 N.3

ISSN 1517-7076 articles e20240161, 2024

Sustainable self-consolidating green concrete: neural-network and fuzzy clustering techniques for cement replacement

Duraimoni Neguja[1], Agniraj Senthilrajan[1]

[1]Alagappa University, Department of Computational logistics. Tamil Nadu, India.

e-mail: neguja@gmail.com; agni_senthil@yahoo.com

ABSTRACT

This study investigates the properties of self-consolidating green concrete (SCGC) through experimental tests and employs artificial intelligence techniques for design parameter analysis. Cement is partially substituted with granulated blast furnace slag (GBFS) powder, volcanic powder, fly ash, and micro-silica. Fresh and hardened properties tests are conducted. An adaptive neuro-fuzzy inference system (ANFIS) is developed to identify parameters influencing compressive strength. Seven ANFIS models evaluate input parameters individually, while twenty-one models assess different input combinations for optimization. Furnace slag significantly impacts hardened properties in binary mixes, while volcanic powder enhances slump retention. Ternary mix design with micro-silica and volcanic powder demonstrates substantial improvement. ANFIS results highlight binder content as the primary governing parameter for SCGC strength. The combination of micro-silica and volcanic powder exhibits superior strength compared to other additives, confirmed by test results. Overall, the study underscores the efficacy of incorporating micro-silica and volcanic powder for enhancing SCGC strength and sustainability.

Keywords: Absorption; Durability; Fly ash; Gypsum; Quarry dust.

1. INTRODUCTION

Global warming prompts researchers to seek emission-cutting alternatives. Cement, a major greenhouse gas emitter, attracts focus for sustainable solutions [1]. Self-consolidating concrete (SCC) is highly dependent on cement, which significantly contributes to its carbon footprint. In response to this issue, academics are actively exploring environmentally acceptable alternatives to decrease reliance on cement. Although SCC has rheological advantages in its initial condition, it also presents difficulties such as excessive cement usage, segregation, and decreased viscosity. [2, 3]. Both natural and synthetic substitutes can be produced concurrently in powder and aggregate formats, or individually as either powder or aggregate [4–6].

Numerous alternatives to traditional cement and aggregates have been suggested, encompassing a diverse spectrum of properties and attributes [7]. Research on waste glass impact on mechanical properties, particularly compressive strength, reveals a gradual decrease in concrete strength with higher waste glass content [8]. Moreover, enhancing the workability and strength of self-consolidating concrete (SCC) entails determining the optimal replacement dosage for crushed waste glass, which has been found to be 20% of the coarse aggregate [9]. When incorporating marble powder, the compressive strength of concrete typically diminishes once the marble powder content surpasses 5%. This highlights the critical threshold for maintaining optimal compressive strength in concrete mixtures containing marble powder [10]. Furthermore, the use of marble powder increases the amount of water required in concrete compositions. Nevertheless, accurately measuring the effect of marble aggregates on the mechanical characteristics of concrete presents difficulties, requiring additional research to thoroughly evaluate their impact on the structural performance [11]. Research has demonstrated that the addition of basalt powder to concrete improves its strength, ductility, and ability to absorb energy, particularly at high temperatures. The optimal replacement level of basalt powder is 2% [12]. Nevertheless, basalt powder is susceptible to extreme conditions such as chloride attacks and direct exposure to flames [13]. Moreover, wood byproducts such as woodchips, wood fiber, and sawdust have the potential to be utilized in creating a recycling system that is environmentally sustainable. One instance is when porous concrete containing clay–cement–wood particles was shown to have a decreased ability to absorb water through capillary action [14].

Corresponding Author: Duraimoni Neguja Received on 06/04/2024 Accepted on 06/05/2024

DOI: https://doi.org/10.1590/1517-7076-RMAT-2024-0161

Adding coconut fiber in concrete enhances mechanical properties. At 2% content and 50mm length, compression and split tension strength improve [15]. With higher coconut fiber content, modulus of elasticity increases [16]. Studies suggest that integrating ceramic waste into concrete and mortar can greatly impact their properties. Partially substituting sand with waste fine aggregate affects mortar workability due to water absorption during ceramic waste preparation. Concrete containing up to 50% fine ceramic aggregates in place of natural aggregates exhibits improved compressive strength and durability. Additionally, incorporating up to 40% ceramic waste as coarse aggregates in high-performance concrete substantially reduces autogenous shrinkage. These findings underscore the potential of ceramic waste as a sustainable alternative in construction materials, offering enhanced mechanical performance and addressing environmental concerns associated with waste disposal [17, 18]. The integration of rubber in concrete, replacing up to 7.5% of the fine aggregate, resulted in a drop in the intended strength of the concrete. As the amount of rubber employed grew, the compressive strength of the concrete fell. Rubberized concrete derives enhanced strength from the inclusion of magnesium oxychloride cement, which imparts advantageous adhesive qualities to rubber and ultimately enhances the performance of the rubber-concrete composite [19, 20]. Substituting rubber tree seeds for 4% of aggregates markedly enhanced concrete performance in the concrete mixture [21]. While waste plastic fibers (WPFs) reduce compressive strength, they enhance flexural strength and ductility when replacing aggregates. Longer PET fibers result in greater flexural capacity. However, utilizing PET fibers and WPAs reduces split tensile strength, with increased fiber content exacerbating this tensile strength loss [22, 23]. The use of PET fibers successfully inhibited the spread of cracks during load-deflection testing, whereas WPFs strengthened and enclosed the connections between internal components [24]. Steel fibres improve mechanical properties in diverse concrete types. Wire SF, sourced from discarded tires, offers another reinforcement option. Incorporating wire SF boosts concrete flexural strength in direct correlation with the quantity of high wire fiber employed [25]. Crack propagation diminishes and strength properties typically enhance with steel fibers (SF). Incorporating 10% micro-silica and 1% SF elevates compressive and flexural strength by 19% and 61%, respectively. Meanwhile, 1.5% SF with 15% fly ash boosts compressive and flexural strength by less than 10% and 35% [26, 27]. Paste cohesiveness and bond behaviour were much improved and crack propagation was effectively limited by the use of waste steel lathe and lathe scrap fibber [28].

Various factors influence self-consolidating concrete (SCC) properties, with the use of supplementary cementitious materials (SCM) being significant. Determining the primary factor affecting SCC properties in SCM-based mixes could lead to optimized designs. Numerous studies explore SCM use in SCC, aiming to establish correlations meeting specific requirements. According to ASTM C618, pozzolans are defined as siliceous or aluminosiliceous materials that, when combined with water and calcium hydroxide, serve as binders, highlighting their crucial role in SCC formulations [29, 30]. Pumice, an igneous rock, serves as a natural pozzolan, enhancing both early- and long-term concrete strength. Processed pumicite (VP) also exhibits remarkable resistance against sulphate attacks. Ground granulated blast furnace slag (GGBFS) functions akin to cement but with significantly lower environmental impact when utilized as a supplementary cementitious material (SCM) [7, 31–33]. GGBFS reduces hydration heat, boosts strength, enhances impermeability, and fortifies resistance to sulphate attacks. Micro-silica improves durability, reduces thermal cracking, and enhances overall engineering properties of concrete. [4, 5]. Using FA enhances workability, promotes binder hydration, and reduces hydration heat in concrete mixtures. [34, 35]. SCMs enhance numerous concrete properties. Incorporating MS notably enhances mechanical and durability characteristics. However, challenges like high cost, limited availability, dispersion issues, and increased water demand limit its use above 5% [36, 37]. This study employed factor analysis as a standard to evaluate the effectiveness of volcanic pozzolan, ground granulated blast furnace slag, and metakaolin as supplementary cementitious materials in self-consolidating concrete. FA is classified according to its chemical composition, particle fineness, and strength activity index in ASTM C618 [38]. This classification allows for reliable comparisons with Portland cement.

Concrete characteristics have been evaluated numerically using diverse methods, spanning classical mathematical algorithms to intelligent-based ones. In this study, the Wiener approach was employed to assess the reliability index of concrete. However, this method encountered challenges due to the presence of non-linear relations within the concrete properties. Despite its limitations, the Wiener approach provides valuable insights into concrete reliability. Researchers continue to explore alternative numerical methods, striving to overcome the complexities posed by non-linear behavior in concrete characteristics assessment. Intelligent algorithms can effectively address non-linear problems and are particularly valuable for solving actual stochastic challenges [1]. A neural network that uses a fuzzy logic algorithm to analyze data is called an adaptive neuro-fuzzy inference system (ANFIS). It has the capability to automatically acquire knowledge and adjust to the facts [39]. ANFIS has been utilized in a wide variety of applications, one of which is the estimate and identification of multivariate systems in real time [40]. In contrast to the majority of analytical processes, ANFIS does not rely on the parameters of the system currently being known [41]. Because it takes a more straightforward approach, it can be utilized in multivariate systems if there is a small amount of input data. When SCC is partially replaced by SCMs, the properties of the concrete are altered. For instance, a change in the compressive strength might occur as a function of time. This is one example of how the concrete qualities are altered [41, 42]. The degree of this change is difficult to quantify, which is a challenge. For this reason, the application of artificial intelligence (AI) to measure the amount of change is also a valuable as well [43]. Within the scope of this investigation, the application of ANFIS will be utilized to assess the impact of various elements that have an impact on the results of SCC properties.

This research investigates the development of sustainable self-consolidating green concrete (SCGC). The focus is on replacing Portland cement (PC) with greener alternatives: volcanic powder (VP), ground granulated blast furnace slag (GGBFS), micro-silica (MS), and fly ash (FA). The study explores binary mixtures (10–50% PC replacement) and ternary mixtures incorporating both MS and VP.Key properties of the SCGC are evaluated, including slump flow (workability), compressive strength, water absorption (durability), and electrical resistivity. To understand the influence of different materials on compressive strength, 28 different Artificial Neural Network-Fuzzy Inference System (ANFIS) models were developed. These models analyzed the impact of individual and combined material factors like VP, GGBFS, MS, FA, and PC content. Finally, the research ranked these material factors along with the measured properties (compressive strength, electrical resistivity, and water absorption) for further analysis.

2. MATERIALS AND METHOD

2.1. Materials

The physical and chemicl properties of the materiels used in this resarch were placed in Tables 1 and 2. In this experiment VP, FA, GGBS and MS are used as the sourse materioel of SCMs for replacing ordinary portland cemnt as well as formation of differnt binary and ternary mixtures.

Table 1: Physical properties of the materials.

MATERIALS	PARTICLE SIZE (AVG)	% OF WATER ADSORBTION	SPECIFIC GRAVITY	DENSITY (BULK) (kg/m^3)	SPECFIC SURFACE AREA (kg/m^2)
OPC	53 µm	–	3.12	1432.00	223.00
Coarse aggregate (Conv)	20 mm	0.8	2.59	1498.00	–
Sand	–	4.23	2.57	1630.00	–
Fly Ash	63 µm	–	2.42	716.00	176.00
GGBS	37 µm	–	2.84	1230.00	462.00
Volcanic powder (VP)	26 µm	–	3.14	2316.00	376.00
Micro silica (MS)	138 nm	–	2.18	686.00	186.00
Hiigh-range water reduc-ing admixture (HWRA)	–	–	1.25	-	

Table 2: Chemical composition of the materials.

MATERIALS	SiO_2	Al_2O_3	Fe_2O_3	CaO	MgO	SO_3	LOI
Fly ash	62.72	32.23	1.06	1.64	0.78	0.47	1.01
GGBS	32.45	14.26	3.73	40.62	7.32	0.64	0.98
Micro-silica (MS)	87.42	2.42	1.87	4.67	0.89	0.37	2.36
Volcanic powder (VP)	57.62	17.72	2.84	13.07	3.96	0.94	1.85
Cement	22.42	4.52	3.76	64.21	2.57	1.42	1.10

To comply with the grading requirements outlined in IS: 383, both coarse and fine aggregates were sieved according to the code's specifications. The fine aggregate particles specifically met the criteria for grading zone II. Figure 1 illustrates the grading curve for both the fine and coarse aggregates.

2.2. Mix proportions

Cement was partially replaced with fly ash (FA), volcanic pumice (VP), and ground granulated blast furnace slag (GBFS) at different proportions ranging from 10% to 50% in binary mixes. In ternary mixtures, VP was used at 25%, 40%, and 45% together with metakaolin (MS) at 5% and 10%. The water to binder ratio was always maintained at 0.38, and the content of cementitious material was kept at 500 kg/m^3 for all designs. The specific weight of the mixture was 2350 kg/m^3. The dry components were initially combined, and then water and HWRA were added in accordance with the IS 9103: 1999 requirements. Slump flow tests, according to EFNARC regulations, were performed right after the mixing process and lasted for 50 minutes. The specimens, shaped into 150mm × 150 mm × 150 mm cubes, were examined at specific time intervals following the guidelines of IS 516:1959, with three specimens each sample.

2.3. Specimen prepration

In each series of mix designs, there are 12 standard cube specimens, with dimensions of 15 × 15 × 15 cm^3, as shown in Figure 2. These specimens are carefully molded within a 24-hour timeframe under controlled laboratory conditions following the mixing procedure. Subsequently, they undergo immersion in lime-saturated water tanks to facilitate further curing. The water tanks maintain a consistent temperature environment, with an average temperature of 23 ± 2°C, ensuring optimal curing conditions for the specimens. Detailed mix proportions for both the binary and ternary mixtures are provided in Tables 3 and 4, respectively, outlining the precise composition of each mixture, including the proportions of cementitious materials and other additives used in the formulation.

2.4. Detailed methodalgy of ANFIS

2.4.1. Prepration of statistical data

Throughout the investigation, a total of 109 compressive strength tests were performed, with their outcomes integrated into the ANFIS models. The inputs and outputs of these models are outlined in Table 5, providing a comprehensive overview of the variables and corresponding responses utilized within the analytical framework. This amalgamation of empirical data and modeling facilitates a deeper understanding of the relationships

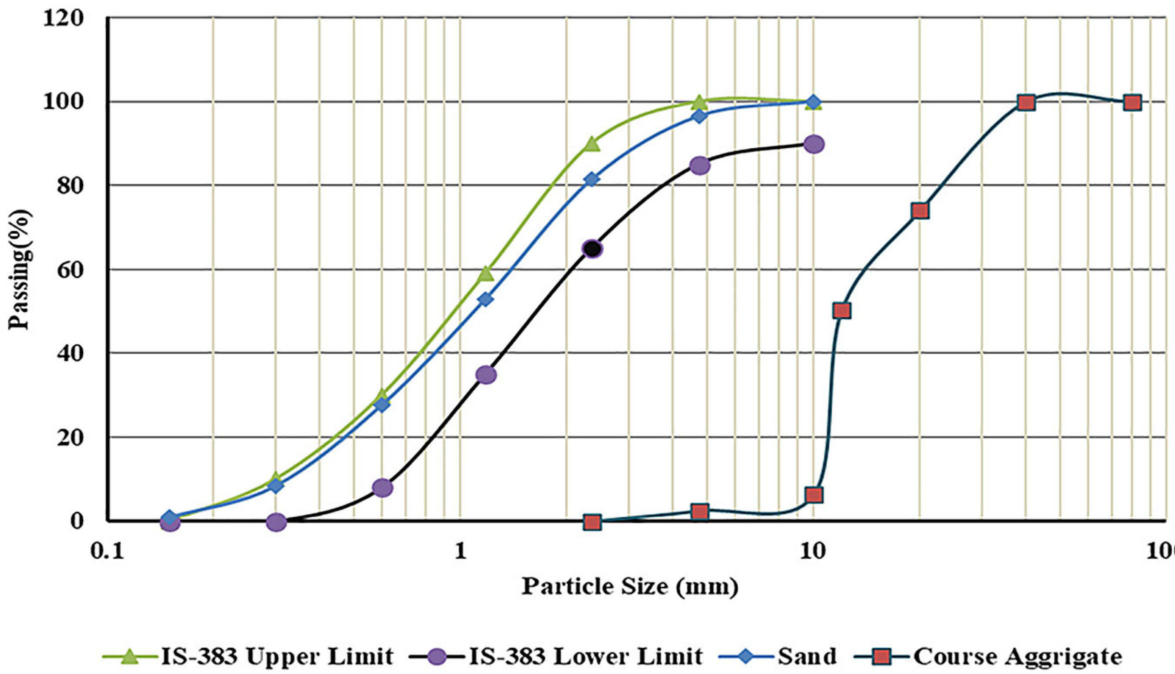

Figure 1: Grading curve of fine and coarse aggregate.

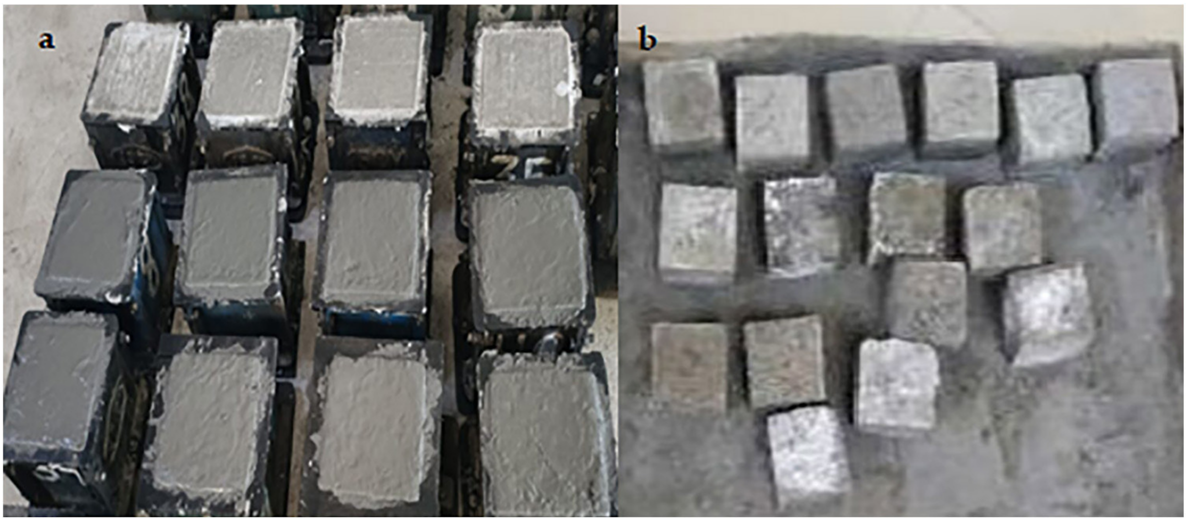

Figure 2: Specimens for cube test.

Table 3: Bineray mix binder of SCC.

SPECIMEN	AGGREGATE (kg/m^3)		BINDER (kg/m^3)				
ID	COARSE	FINE	CEMENT	VOLCANIC PUMICE (VP)	MICRO SILICA (MS)	GGBS	FLY ASH (FA)
10GGBS.	1080	594	455	–	–	50.	–
20GGBS.	1070	593	405	–	–	100.	–
30GGBS.	1065	594	355	–	–	150.	–
40GGBS.	1060	592	302	–	–	200.	–
50GGBS.	1070	585	255	–	–	250.	–
10VP.	1080	595	455	.50	–	–	–
20VP.	1070	595	405	.100	–	–	–
30VP.	1065	590	355	.150	–	–	–
40VP.	1060	595	302	.200	–	–	–
50VP.	1070	590	255	.250	–	–	–
10FA.	1065	595	455	–	–	–	50
20FA. .	1050.	585	405	–	–	–	.100
30FA..	1045.	580	355	–	–	–	.150
40FA..	1030	570	302	–	–	–	.200
50FA..	1020	565	255	–	–	–	.250

Table 4: Ternary mix binder of SCC.

SPECIMEN	AGGREGATE (KG/M^3)		BINDER (kg/m^3)		
ID	FINE	COARSE	CEMENT	VOLCANIC PUMICE	MICRO-SILICA
VP5-MS5..	1065	579	450	25	25
.VP10-MS10.	1050	584	400	50	50
.VP25-MS5.	1040	582	350	125	25
.VP30-MS10.	1065	593	300	150	50
VP40-MS10.	1050	585	250	250	50
VP45-MS5..	1050	580	250	225	25

between various factors and the resulting compressive strength, contributing to the overall robustness and effectiveness of the ANFIS approach employed in the study.

2.4.2. Architure of ANFIS

The Adaptive Neuro-Fuzzy Inference System (ANFIS) has emerged as a potent methodology within the realm of engineering studies, harnessing the amalgamation of fuzzy logic principles within neural network frameworks. This innovative approach has found widespread application across diverse prediction and evaluation domains. Initial exploration of datasets often reveals unpredictable patterns or nonlinear relationships, rendering direct application of algorithms on such "crisp data" impractical. Consequently, the fuzzy method provides a solution by transforming crisp data into a fuzzy inference engine through a fuzzifier step. This pivotal stage initiates the fuzzification process within the system, wherein data is converted into fuzzy sets, enabling nuanced representation of uncertainties and vagueness inherent in real-world datasets. Subsequently, the system navigates through computational processes, leveraging the principles of fuzzy logic to infer relationships and patterns embedded within the data. Notably, the predicted outcomes are refined back into a crisp state through a process termed as DE fuzzifier, ensuring interpretability and applicability of results in practical engineering contexts. Figure 3 serves as a visual aid, delineating the intricate stages involved in the fuzzification process integral to the fuzzy technique. Through the seamless integration of fuzzy logic and neural network paradigms, ANFIS empowers engineers and researchers to tackle complex, real-world problems characterized by uncertainty and nonlinearity, facilitating more robust and informed decision-making processes across various engineering applications.

The ANFIS network, which consists of five layers, is shown in Figure 4, with the fuzzy inference system acting as its hub. Layer 1 is in charge of taking inputs and using membership functions to convert them into fuzzy values. Because bell-shaped membership functions are better at regressing nonlinear data, they were used in this experiment. By making it easier to transform input data into fuzzy sets, these functions help the network better capture the underlying uncertainties and complexities included in the dataset. The ANFIS network's capacity to manage nonlinear interactions and produce precise predictions, thanks to the use of bell-shaped membership functions, increases its application in engineering investigations.

Table 5: Input and Output.

INPUTS	OUTPUT	PARAMETERS DESCRIPTION	PARAMETERS DESCRIPTION
Input -1.		.Volcanic powder (kg/m^3)	
Input- 2.		.Micro-silica (kg/m^3)	
Input -3.		.Fly ash (kg/m^3)	
Input -4.		Furnace slag (kg/m^3)	
Input -5.		.Electrical resistivity (ohm-meter)	
Input -6.		.Water absorption (%)	
Input -7		.Cement (kg/m^3)	
	Output		Compressive strength (MPa)

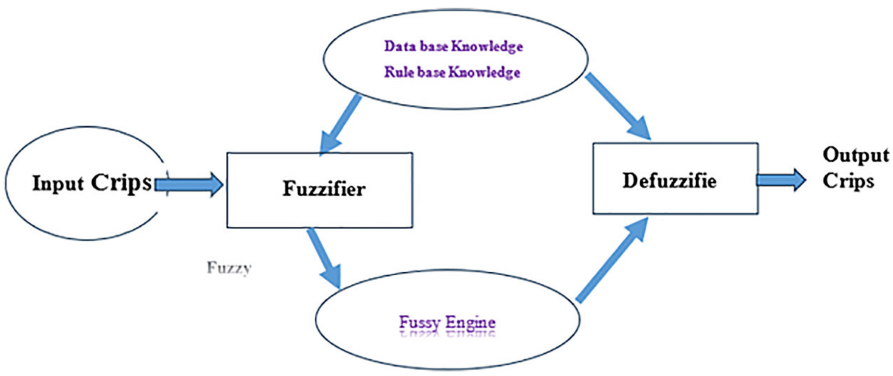

Figure 3: ANFIS algaritam for fuzzification.

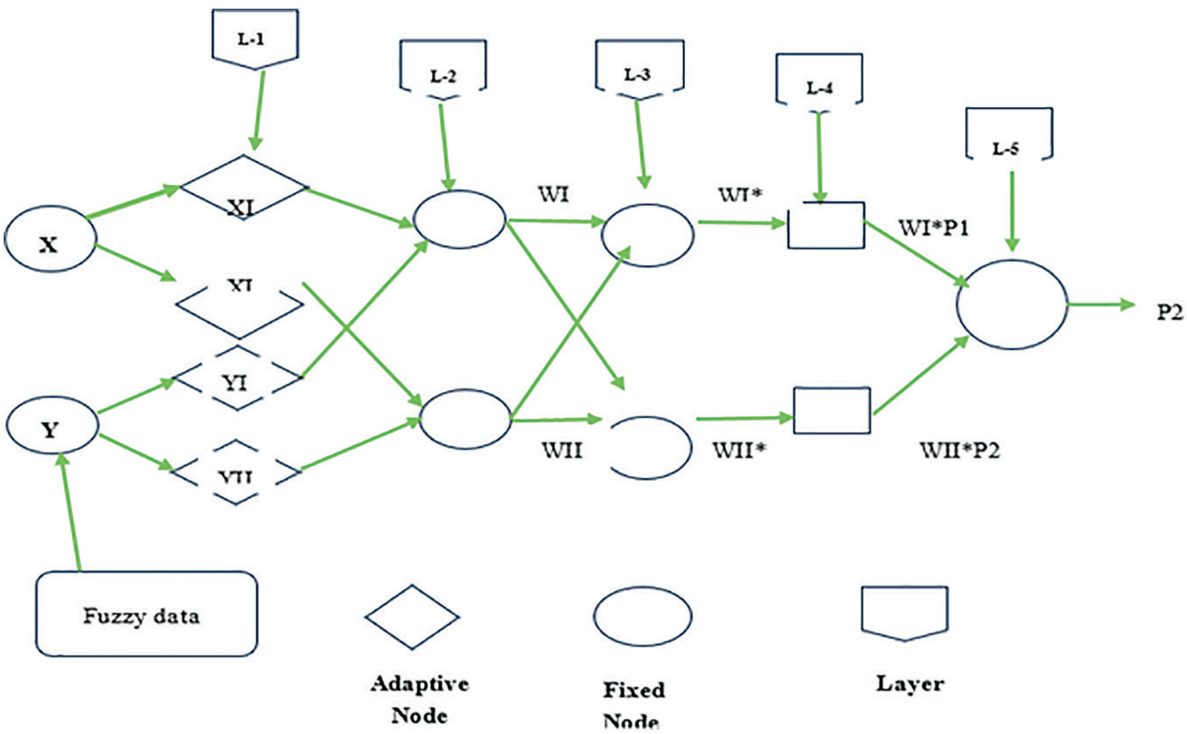

Figure 4. Different layers of ANFIS.

The definition of the bell-shaped membership function is as follows:

$$\mu x = bellx;at,bt,ct = 11 + \times\text{-}ctat2bt \qquad (1)$$

where {, , , }are the parameters set and x is the input.

In the ANFIS network, the second layer calculates the firing strength of each rule by multiplying the fuzzy signals received from the first layer. Subsequently, the third layer, known as the rule layer, normalizes all signals obtained from the second layer. Following this, in the fourth layer, the inference of rules occurs, where the normalized signals are used to make inferences, leading to the conversion of all signals into crisp values. Finally, the fifth layer aggregates these signals to generate a crisp output value.

The procedure of variable identification utilized a hybrid learning algorithm. The functional signals are processed up to the fourth layer, at which point the hybrid learning method is implemented across all levels. The method of least squares was utilized to derive the resulting variables. On the other hand, for the backward path, the error rate travels in the other direction and follows a decreasing gradient order, while the premise variables are synchronized.

2.4.3. Identification of different parametes

The ANFIS network is first trained for each input to identify the parameters. Then, the combination of inputs is taken into account [44]. The impact of each input on the output can be assessed by the magnitude of Root Mean Square Error (RMSE), which is a well recognized criterion for measuring accuracy [45]. RMSE, or Root Mean Square Error, is a forecasting metric that quantifies the performance of the constructed network [46]. The parameter mentioned above is defined by the equation [47].

$$RMSE = q = 1q = z(Pq–Oq)2z \qquad (2)$$

where and are the predicted and observed variables, and z is the total number of considered data.

In order to assess the effectiveness of parameters in the numerous ANFIS models developed, Root Mean Square Error (RMSE) was employed as a metric. To ensure robustness, 70% of the data was randomly allocated for training purposes, with the remaining 30% reserved for testing. Throughout both the training and testing phases of the ANFIS models, MATLAB 2019 fuzzy inference system was utilized. It's essential to note that any interventional studies involving animals or humans, as well as other ethically approved investigations, must explicitly state the approval authority and corresponding code for ethical clearance.

3. RESULT AND DISCUSSION

3.1. Slump

Concrete was prepared to achieve a slump flow of 650 ± 25 mm, per EFNARC committee recommendation. This was done with varied HWRA quantities [48, 49]. IS199 criteria were used to evaluate new self-consolidating concrete (SCC) workability by measuring slump flow at 10, 20, 30, 40, and 50 minutes [5]. The self-consolidating concrete (SCC) was separated into five slump cones once its first slump flow proved acceptable. The slump flow test was then done at 5, 23, and 43 minutes. After the initial slump flow test, a slump cone was lifted every 10 minutes for 50 minutes. We measured slump flow with 5 cones for each mixture. To improve precision and validity, the tests were repeated four times with different percentages, returning the same result. Stir the liquid for 20 seconds before each test.

This test assesses the extent to which concrete spreads after the removal of a funnel, and the resulting data indicates the level of filling capacity and stability of self-consolidating concrete. The slump flow of the specimens containing VP, evaluated throughout the time range of 3 to 50 minutes, is displayed in Figure 3. Additional slump values can be found in Table 6.

Figure 5 shows that, except for the VP 10% sample, not all mixtures reached the required slump within 3 minutes. However, by 10 minutes, all achieved suitable values, possibly due to HWRA mixing. VP usage notably

Table 6: Slump values of SCC mixures.

SPECIMEN	SLUMP VALUE (cm) WITH RESPECT TO TIME					
	3 minutes	10 minutes	20 minutes	30 minutes	40 minutes	50 minutes
.Ctrl-FA	51	63	61	59	53	49
.FA10	65	63	62	60	58	55.5
.FA20	45.5	63.5	62.5	59.5	58.5	56
.FA30	54	65	61.5	59.5	56.5	54
.FA40	51	64	59	58	55	53.5
.FA50	55.5	62	60.5	56	54.5	51.5
.Ctrl-GBFS	41	63.5	58.5	54	52.5	49.5
. .GBFS10	68	65.5	62.5	54.5	55.5	52.5
.GBFS20	67	65.5	61.5	58	56.5	54.5
.GBFS30	57.5	64.5	61	57.5	55.5	53
.GBFS40	64.5	63.5	62	58.5	53.5	51.5
.GBFS50	57.5	63.5	62.5	61	58	56
.Ctrl-VP	52.5	64	62.5	60.5	59.5	53
.VP10	66.5	66.5	64	62	60	58
.VP20	45	63.5	65.5	63.5	61.5	59.5
.VP30	54.5	63.5	64	63	61	59
.VP40	52	65	66	67	63	60
.VP50	53.5	64.5	65.5	67.5	64.5	60
.Ctrl-ternary	52.5	62.5	57.5	56	53.5	52
.VP5-MS5	54.5	64	62	58.5	54.5	49.5
.VP10-MS10	52.5	64.5	59.5	54.5	49.5	42.5
.VP25-MS5	58.5	63.5	58.5	54.5	55	52.5
.VP30-MS10	61	64.5	65.5	61.5	59	55.5
.VP40-MS10	44.5	64	60.5	56.5	53.5	48
.VP45-MS5	51.5	63.5	64.5	63	52	51

retained slump values, with increasing VP content correlating with increased retention. The bell-curve trend in slump flow may be attributed to VP's water absorption and release properties. This aligns with HOSSAIN and LACHEMI [50], indicating increased slump and entrapped air with higher VP content, affecting workability and compressive strength.

Table 6 shows varying slump values, with GBFS specimens exhibiting the most, especially at 50% replacement, indicating superior slump retention. GBFS, with lower-paste viscosity and less water-soluble glass crystalline particles than VP, enhances slump. BHEEL *et al*. [51] noted decreased workability due to porous GGBFS and FA particles absorbing more water with higher percentages. Additionally, BHEEL *et al*. [52] confirmed increased workability with greater VP substitution for Portland cement.

Figure 6 and 7 reveal a contrasting trend for FA, with increasing amounts leading to more slump loss, likely due to its fine particle size compared to cement, VP, and GBFS. MS, with the smoothest particles, enhances slump, particularly in ternary mixes, where VP and MS increase slump up to 30% and 10%, respectively. Despite expectations of further slump reduction with increased MS, VP presence ensures suitable slump retention, notably in VP30-MS10 mix.

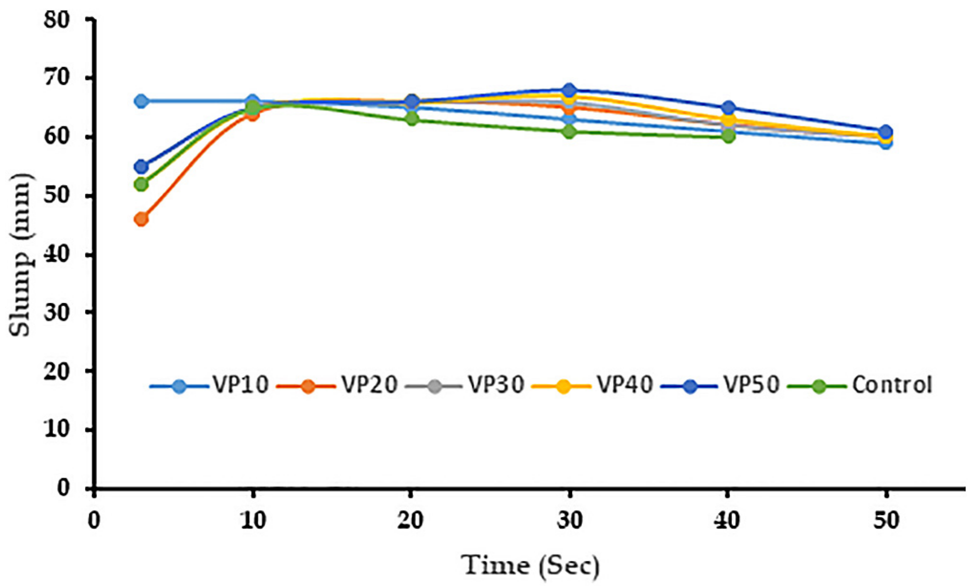

Figure 5: Slump value of SCC on VP dosage.

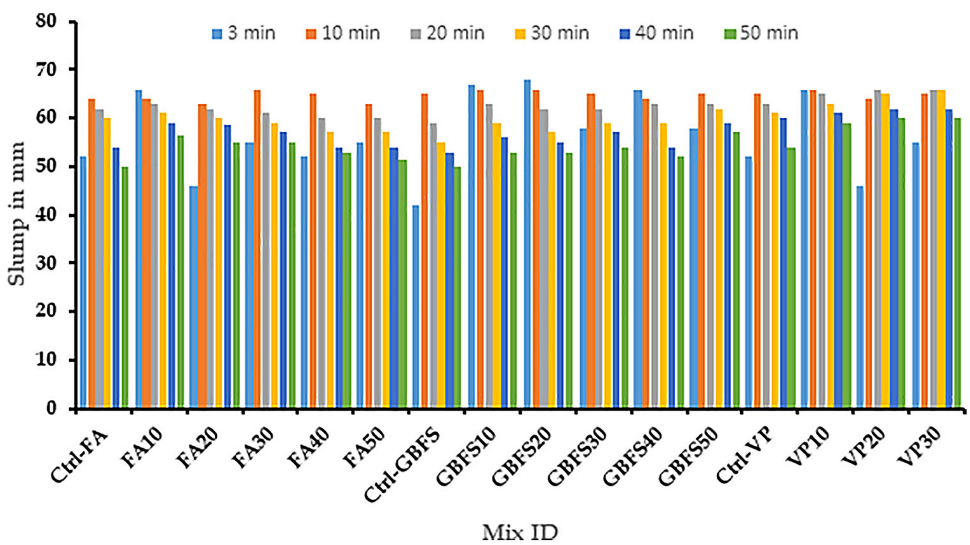

Figure 6: Slump value binary mix samples.

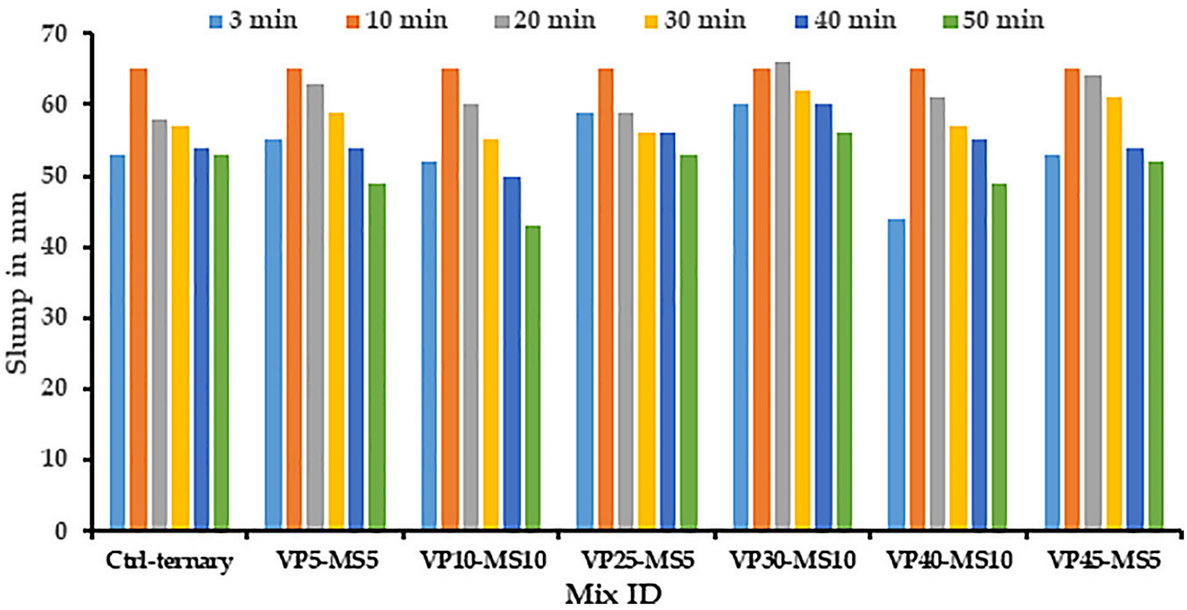

Figure 7: Slump value ternary mix samples.

3.2. Mechanical properties of SCC

3.2.1. Compressive stregth

Compressive strength testing was conducted in accordance with IS 516: 1959 [53]. Specimens were tested at 7, 28, and 90 days, and the results are presented in Table 7. Figure 8 depicts a specimen undergoing the compressive strength test.

The quantities of SiO_2 and Al_2O_3, outlined in Table 2, are crucial chemical factors affecting compressive strength in cementitious materials. FA boasts the highest Al_2O_3 content, while MS contains the most SiO_2. Consequently, these powders are expected to significantly enhance compressive strength [54]. However, Figure 9 indicates that as FA replacement percentage increases, compressive strength decreases. At 28 days, there's a 30% strength loss between 0% and 50% FA replacement, with a steady decline up to 30% replacement, followed by a sharp drop. This behavior is attributed to FA reacting with $Ca(OH)_2$ in concrete paste, forming adherent components. $Ca(OH)_2$, a byproduct of C_3S hydration, decreases with increasing FA replacement, impacting concrete's mechanical properties. Results show that up to 30% replacement, $Ca(OH)_2$ presence is sufficient, but a further 10% reduction dissipates $Ca(OH)_2$, leading to sudden compressive strength reduction. Binary mixtures are expected to exhibit higher strength over time due to the pozzolanic reaction, enhancing the microstructure of hardened cement [35]. Compressive strength of binary mixtures at older ages (90 days) approaches that of control specimens, evident in Figure 10.

In Figures 9, 10, and 11, VP and FA exhibit similar trends in compressive strength reduction with increasing replacement percentages. At 90 days, no significant difference is observed up to 30% replacement. VP demonstrates more efficient strength development compared to FA, as indicated by a relatively lower strength loss (22% vs. 30% for FA at 50% replacement). Studies by HANS. S et al., [55] and KARRI *et al*. [56] highlight the strength-enhancing effects of GGBFS substitution in concrete. RAMAN and KRISHNAN [57] found that 40–50% GGBFS yielded the highest compressive strength, while investigations by HOSSAIN and ROCHA *et al*. [58, 59] noted a reduction in compressive strength with VP substitution.

Figure 4, 5, and 6 suggest that GBFS, closely resembling cement, yields higher compressive strength gains in binary mixes. At 10%, 20%, and 30% replacements, strengths match the control specimen, with only a 9% reduction at 50% replacement, contrasting with 22% and 30% reductions for VP and FA, respectively.

Figure 11 presents 90-day compressive strength results converted to relative percentages for comparison. GBFS demonstrates the most significant impact, attributed to its larger surface area facilitating ion penetration and its high SiO_2 and CaO content enhancing mechanical properties. Binaries show delayed strength development, suggesting additional time is needed. Consequently, ternary mixtures of VP with micro-silica were explored to enhance compressive strength and durability, detailed in Table 7 and Figure 12.


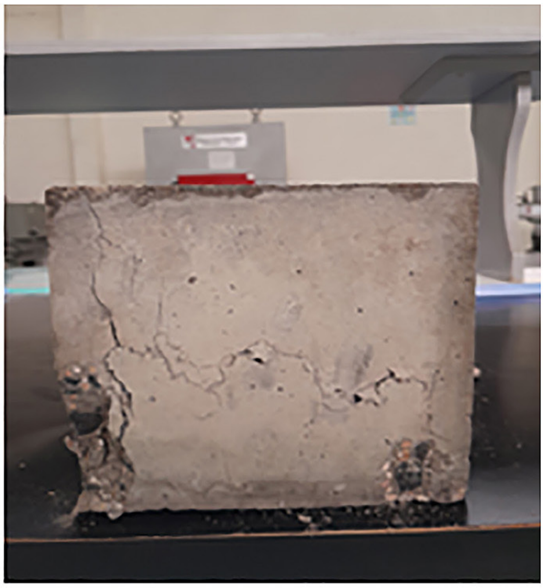

Figure 8: Experimental set up and tested samples.

Table 7: Compressive of SCC mixures.

SPECIMEN ID	COMPRESSIVE STRENGTH (Mpa)		
	7th day	28th day	90th day
.Ctrl-FA	.31.74	.46.73	.55.31
.FA10%	.29.37	. .46.62	.53.16
.FA20%	.26.28	45.35	.51.55
.FA30%	.25.27	.43.07	.50.09
.FA40%	.23.11	.36.11	.48.42
.FA50%	.15.52	.32.86	.39.07
.Ctrl-GBFS	.36.15	.44.75	.48.92
.GBFS10%	.35.24	.45.24	. .47.35
.GBFS20%	.34.71	.45.83	.49.02
.GBFS30%	.34.53	.46.28	.50.53
.GBFS40%	.31.12	.38.49	.43.14
.GBFS50%	.25.19	.37.47	.44.42
.Ctrl-VP	..31.72	.38.34	.49.35
.VP10%	.31.06	.37.26	.49.02
.VP20%	.29.02	.36.01	..48.81
.VP30%	.23.82	.35.13	.45.82
.VP40%	.21.65	..31.74	.39.09
.VP50%	.16.42	.27.82	.38.72
.Ctrl-ternary	.41.32	.46.65	.48.02
.VP5-MS5	.30.23	..40.23	.46.27
.VP10-MS10	.37.32	.43.81	.49.12
.VP25-MS5	.39.71	.43.08	.54.05
.VP30-MS10	.40.15	.52.41	.59.22
.VP40-MS10	.35.22	.54.01	.58.32
.VP45-MS5	.32.14	.40.87	.51.44

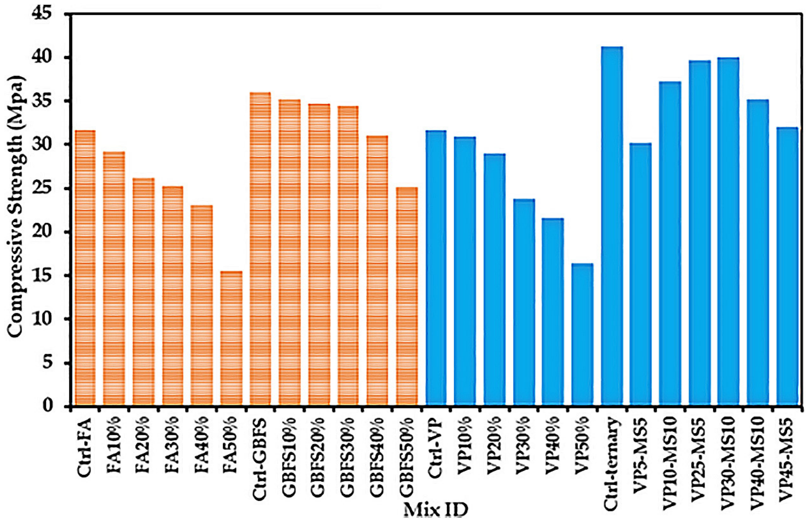

Figure 9: Relative compressive strength of 7th day samples.

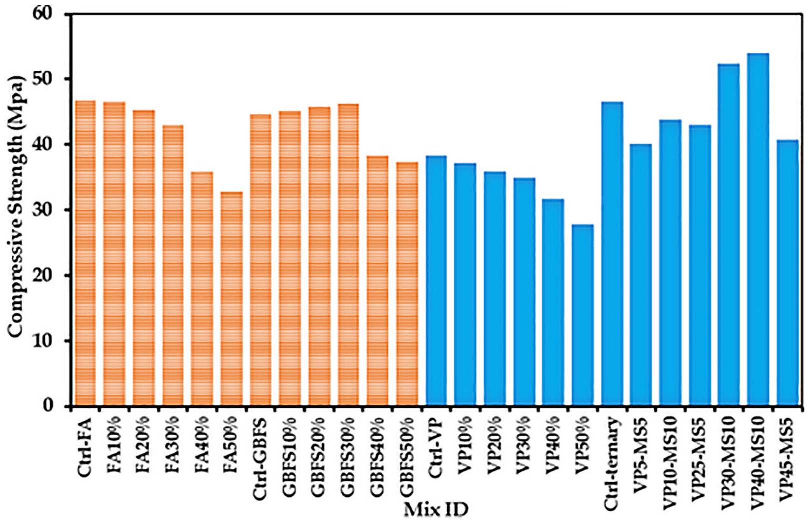

Figure 10: Relative compressive stregth of 28th day samples.

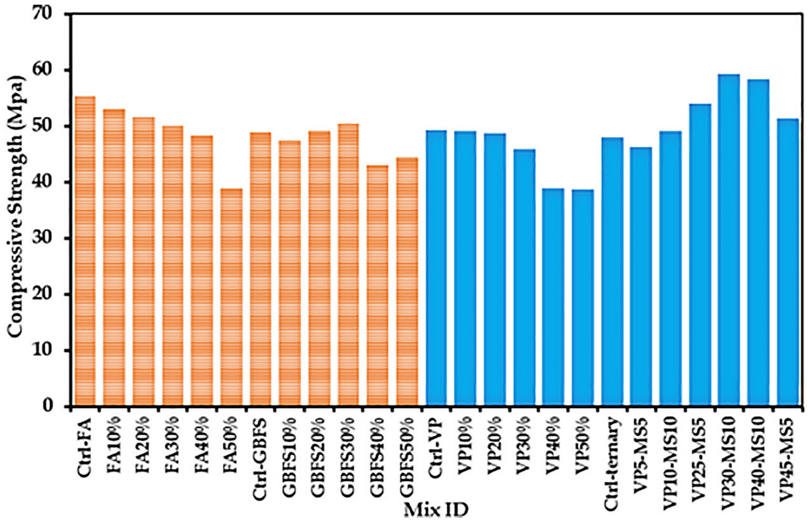

Figure 11: Relative compressive stregth of 90th day samples.

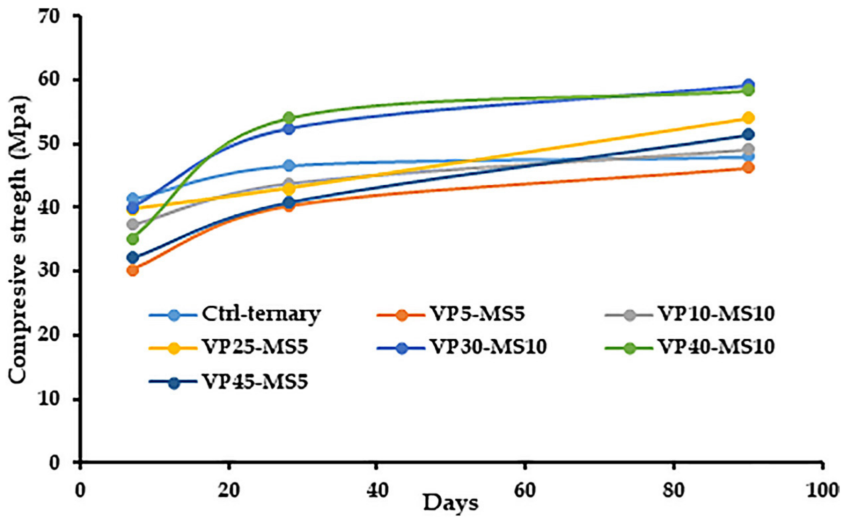

Figure 12: Relative compressive stregth of 7th day samples.

Studies suggest that compressive strength growth can accelerate with 2.5–10% micro-silica replacement [4, 5, 31, 60]. HUNG *et al*. [61] found that GGBFS replacement up to 20% generated a pozzolanic response, enhancing sample compactness compared to the control. Resistivity increased notably with 20% GGBFS introduced later, followed by the 10% GGBFS group. These findings underscore the potential of micro-silica and GGBFS in improving compressive strength and sample compactness.

The early strength varies, with the control having the highest strength and C50-MS5-VP45 having the lowest strength. After 28 days, the compressive strengths of C50-MS5-VP45, C70-MS5-VP25, and C90-MS5-VP5 reach the desired level, while C50-MS10-VP40 surpasses it. After 90 days, the control strength reaches its minimum level, whereas C50-MS10-VP40 demonstrates the highest strength. The presence of a higher lime component in MS increases the cohesiveness between particles [22]. MS granules enhance the strength of the material by filling up the weak areas between the paste and aggregates [46].

Replacing a high volume of particles (VP) reduces the compressive strength within a 90-day period. Preliminary ternary findings indicate that micro-silica is unable to counteract the weakening impact of VP, resulting in all strengths being lower than the control samples. Over time, the addition of micro-silica, together with an increased amount of lime, enhances the strength of the interfacial transition zones, exceeding the strength of the control samples. The development of resistance observed in this investigation is consistent with the study's aims, as it demonstrates the effectiveness of micro-silica even when used in high volumes of volatile particles.

3.3. Results of ANFIS analysis

Table 8 presents the root mean square error (RMSE) values for training and testing for each input. Among them, input 5, which represents electrical resistivity, exhibits the lowest training RMSE. This suggests that electrical resistivity has a noteworthy impact on the output. In contrast, micro-silica (input 2) has the highest training RMSE, most likely because of its combined utilisation with VP, rather than when used independently. The integration of inputs in models emphasises the strong impact of micro-silica, especially when combined with VP (model 8), as demonstrated by the significant decrease in RMSE. The comparisons across ANFIS models highlight the significant impact of micro-silica with VP, among other additional powders, on the compressive strength. Figure 13 demonstrates the close proximity between training and testing RMSE, demonstrating successful network training without overfitting. Table 9 examines the collective impact of input factors on output. Model 11, which includes VP replacements and electrical resistivity, shows a substantial influence.

As a result, Figure 14 shows the regression curve for the created ANFIS prediction, which is associated with Model 5. The r-squared value, or coefficient of determination, is likewise displayed in Figure 15 and is equal to 0.956. In this instance, values that are closer to one indicate that the measured and anticipated values are closely aligned.

Figure 15 illustrates a radar design chart displaying the RMSE values for the predictions of models 8 to 28 throughout the train and test phases. Model 11 exhibits the lowest RMSE. Figure 16 depicts a regression chart

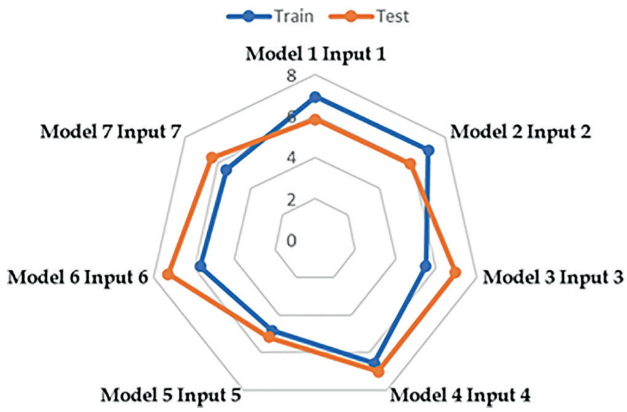

Figure 13: Train and test RSMEs for separate inputs.

Table 8: Root Mean Square Errors (RMSEs) for the individual input parameters during training and testing.

MODEL NUMBER	COMPOSITION	RMSE	
		TRAIN	TEST
Model -1	Input -1	6.9423	5.856
Model - 2	Input -2	7.0045	5.913
Model -3	Input -3	5.4883	6.973
Model -4	Input -4	6.5803	7.031
Model -5	Input --5	4.8234	5.193
Model -6	Input 6	5.6952	7.296
Model -7	Input -7	5.506	6.420

Table 9: RMSEs for the input parameters were calculated during the training and testing phases.

MODEL NUMBER	COMPOSITION	RMSE	
		TRAIN	TEST
Model- 8	Input- 1 & Input -2	5.4473	5.4473
Model -9	Input --1 & Input- 3	5.9736	5.9736
Model -10	Input -1 & Input -4	6.3064	6.3064
Model -11	Input -1 & Input -5	2.1982	2.1982
Model -12	Input -1 & Input -6	4.1475	4.1475
Model -13	Input -1 & Input- 7	4.1713	4.1713
Model -14	Input -2 & Input-- 3	5.4573	5.4573
Model -15	Input 2 & Input -4	5.7363	5.7363
Model- 16	Input -2 & Input -5	4.0771	4.0771
Model -17	Input -2 & Input- 6	9.0073	9.0073
Model -18	Input -2 & Input -7	4.9474	4.9474
Model -19	Input -3 & Input -4	5.5571	5.5571
Model- 20	Input -3 & Input -5	4.0388	4.0388
Model -21	Input -3 & Input -6	4.6874	4.6874
Model -22	Input -3 & Input 7-	4.1893	4.1893
Model -23	Input -4 & Input- 5	4.6573	4.6573
Model -24	Input -4 & Input -6	6.7008	6.7008
Model -25	Input -4 & Input -7	5.5092	5.5092
Model -26	Input -5 & Input- 6	3.478	3.478
Model- 27	Input -5 & Input -7	3.4779	3.4779
Model 2-8	Input -6 & Input -7	3.8576	3.8576

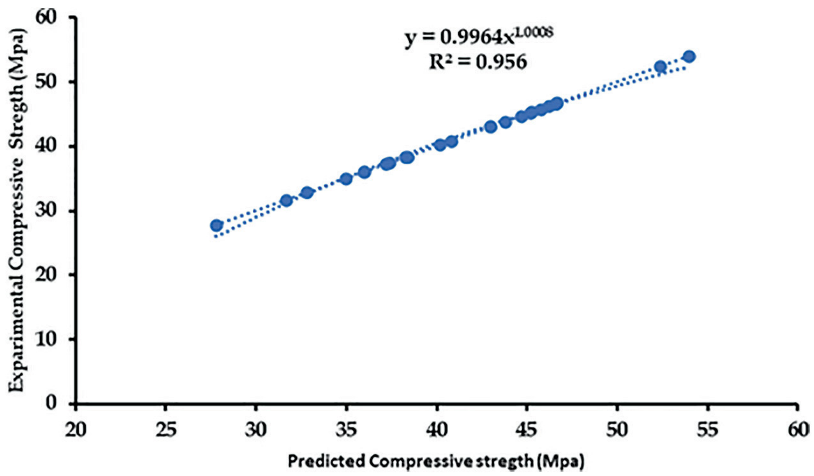

Figure 14: Train and test RSMEs for separate inputs.

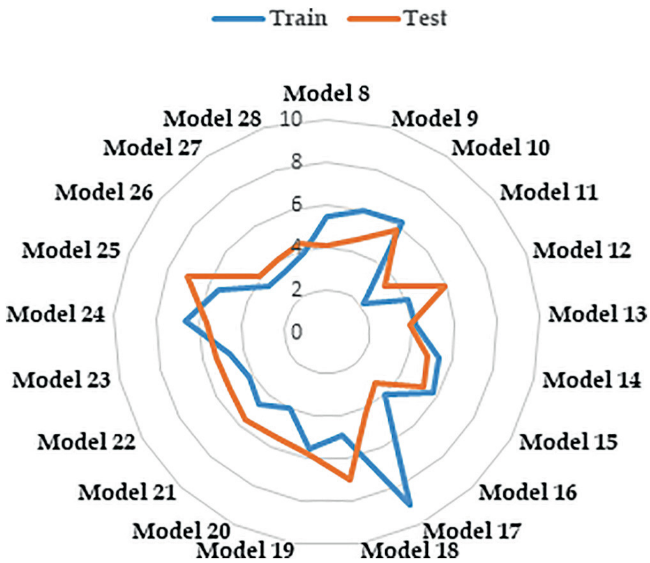

Figure 15: RSMEs for both the training and testing datasets, treating them as distinct inputs.

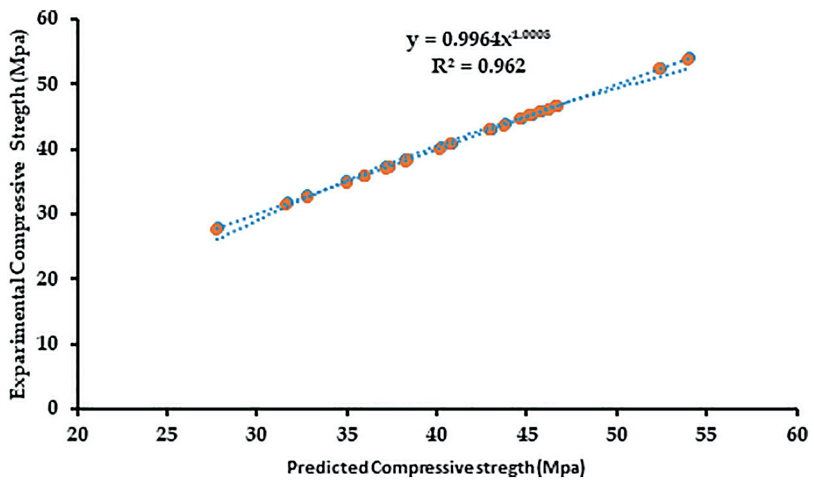

Figure 16: Model 11 train phase regression for compressive strength prediction.

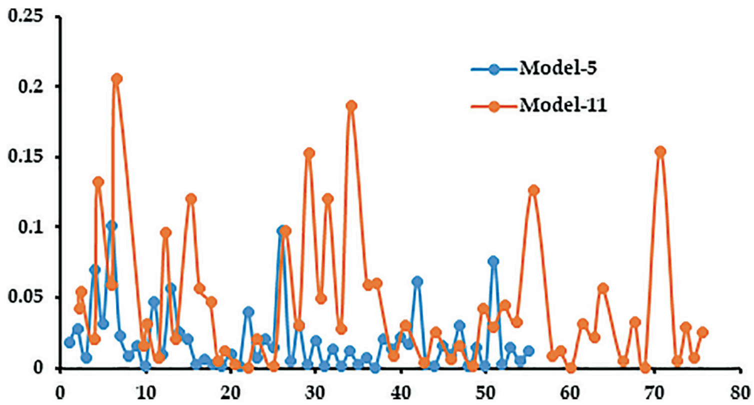

Figure 17: Model 5 and 11 prediction for error.

of the training phase for model 11, showing an r-squared value of 0.962, which indicates a high level of accuracy in predicting outcomes. Furthermore, Figure 17 displays a comparative chart illustrating the level of error between models 5 and 11, so verifying the presence of minimum error and consistent prediction performance throughout the entire process.

4. CONCLUSION

Self-consolidating concrete is popular for concrete structures due to its great formability, segregation resistance, and vibration-free consolidation. Environmental dangers and fluidity difficulties limit concrete manufacturing cement utilisation. Finding a new sustainable mix design with eco-friendly cement substitutes is trendy, thus researchers are studying natural additives in SCGC. This work examined self-consolidating concrete's mechanical properties analytically and experimentally. Binary designs are easier to prepare than ternary ones since they require less precision. The concrete business prioritises eco-efficiency, thus powders, new concrete tests, mechanical qualities, and durability were used to determine the best percentage and economic evaluation. ANFIS was used to assess concrete compressive strength characteristics in a novel way. Seven ANFIS models examined parameter effects. Additionally, 21 different ANFIS models were examined to see how combination characteristics affect SCGC compressive strength when cement is partially substituted by pumice, slag, silica fume, and fly ash. To summarise this paper's findings:

- The volcanic powder greatly influences the maintenance of excellent performance in SCGC slump. Nevertheless, the VP powder has a higher demand for superplasticizer compared to the other two powders.
- GBFS and VP exhibit similar compressive strengths to the control specimen, which favours compressive strength over fly ash in the replacement range of 0–30%.
- The results of the initial seven ANFIS models, in which factors were examined individually, indicate that electrical resistivity has the greatest impact on the compressive strength of SCGC. This is evident from the lowest value of RMSE, which was achieved while considering the input related to cement replacements.
- VP with micro-silica had the greatest influence on concrete resistance in this investigation, according to ANFIS models.The second 21 ANFIS models showed that cement and VP had the greatest impact on SCGC specimen compressive strength by having the lowest RMSE among the coupled parameters.

5. BIBLIOGRAPHY

[1] LIU, J., MOHAMMADI, M., ZHAN, Y., *et al*., "Utilizing artificial intelligence to predict the superplasticizer demand of self-consolidating concrete incorporating pumice, slag, and fly ash powders", *Materials (Basel)*, v. 14, n. 22, pp. 6792, 2021. doi: http://doi.org/10.3390/ma14226792. PubMed PMID: 34832194.

[2] ZEYBEK, Ö., ÖZKILIÇ, Y.O., KARALAR, M., *et al*., "Influence of replacing cement with waste glass on mechanical properties of concrete", *Materials (Basel)*, v. 15, n. 21, pp. 7513, 2022. doi: http://doi.org/10.3390/ma15217513. PubMed PMID: 36363102.

[3] KARALAR, M., ÖZKILIÇ, Y.O., AKSOYLU, C., *et al*., "Flexural behavior of reinforced concrete beams using waste marble powder towards application of sustainable concrete", *Frontiers in Materials*, v. 9, pp. 1068791, 2022. doi: http://doi.org/10.3389/fmats.2022.1068791.

[4] SHARIATI, M., RAFIE, S., ZANDI, Y., *et al.*, "Experimental investigation on the effect of cementitious materials on fresh and mechanical properties of self-consolidating concrete", *Advances in Concrete Construction*, vol. v. 8, n. 3, pp. 225–237, 2019.

[5] ARDALAN, R.B., JOSHAGHANI, A., HOOTON, R.D., "Workability retention and compressive strength of self-compacting concrete incorporating pumice powder and silica fume", *Construction & Building Materials*, v. 134, pp. 116–122, 2017. doi: http://doi.org/10.1016/j.conbuildmat.2016.12.090.

[6] KARALAR, M., BILIR, T., ÇAVUŞLU, M., *et al.*, "Use of recycled coal bottom ash in reinforced concrete beams as replacement for aggregate", *Frontiers in Materials*, v. 9, pp. 1064604, 2022. doi: http://doi.org/10.3389/fmats.2022.1064604.

[7] BOUKENDAKDJI, O., KADRI, E.H., KENAI, S., "Effects of granulated blast furnace slag and superplasticizer type on the fresh properties and compressive strength of self-compacting concrete", *Cement and Concrete Composites*, v. 34, n. 4, pp. 583–590, 2012. doi: http://doi.org/10.1016/j.cemconcomp.2011.08.013.

[8] NAJAF, E., ABBASI, H., ZAHRAI, S.M., "Effect of waste glass powder, microsilica and polypropylene fibers on ductility, flexural and impact strengths of lightweight concrete", *International Journal of Structural Integrity*, v. 13, n. 3, pp. 511–533, 2022. doi: http://doi.org/10.1108/IJSI-03-2022-0039.

[9] ÇELIK, A.İ., ÖZKILIÇ, Y.O., ZEYBEK, Ö., *et al.*, "Mechanical behavior of crushed waste glass as replacement of aggregates", *Materials (Basel)*, v. 15, n. 22, pp. 8093, 2022. doi: http://doi.org/10.3390/ma15228093. PubMed PMID: 36431578.

[10] SHARMA, N., SHARMA, P., PARASHAR, A.K., "Use of waste glass and demolished brick as coarse aggregate in production of sustainable concrete", *Materials Today: Proceedings*, v. 62, pp. 4030–4035, 2022. doi: http://doi.org/10.1016/j.matpr.2022.04.602.

[11] BASARAN, B., KALKAN, I., AKSOYLU, C., *et al.*, "Effects of waste powder, fine and coarse marble aggregates on concrete compressive strength", *Sustainability (Basel)*, v. 14, n. 21, pp. 14388, 2022. doi: http://doi.org/10.3390/su142114388.

[12] REN, W., XU, J., SU, H., "Dynamic compressive behavior of basalt fiber reinforced concrete after exposure to elevated temperatures", *Fire and Materials*, v. 40, n. 5, pp. 738–755, 2016. doi: http://doi.org/10.1002/fam.2339.

[13] SHEN, M., ZHOU, L., CHEN, Z., *et al.*, "Effects of basalt powder and silica fume on ultra-high-strength cementitious matrix: a comparative study", *Case Studies in Construction Materials*, vol. 17, pp. e01397, 2022.

[14] BOUGUERRA, A., AMIRI, O., AÏT-MOKHTAR, A., *et al.*, "Water sorptivity and pore structure of wood–cementitious composites", *Magazine of Concrete Research*, v. 54, n. 2, pp. 103–112, 2002. doi: http://doi.org/10.1680/macr.2002.54.2.103.

[15] ALI, B., HAWREEN, A., KAHLA, N.B., *et al.*, "A critical review on the utilization of coir (coconut fiber) in cementitious materials", *Construction & Building Materials*, v. 351, pp. 128957, 2022. doi: http://doi.org/10.1016/j.conbuildmat.2022.128957.

[16] SHCHERBAN', E.M., STEL'MAKH, S.A., BESKOPYLNY, A.N., *et al.*, "Normal-weight concrete with improved stress–strain characteristics reinforced with dispersed coconut fibers", *Applied Sciences (Basel, Switzerland)*, v. 12, n. 22, pp. 11734, 2022. doi: http://doi.org/10.3390/app122211734.

[17] NAJM, H.M., NANAYAKKARA, O., AHMAD, M., *et al.*, "Mechanical properties, crack width, and propagation of waste ceramic concrete subjected to elevated temperatures: a comprehensive study", *Materials (Basel)*, v. 15, n. 7, pp. 2371, 2022. doi: http://doi.org/10.3390/ma15072371. PubMed PMID: 35407705.

[18] MEENA, R.V., JAIN, J.K., CHOUHAN, H.S., *et al.*, "Use of waste ceramics to produce sustainable concrete: a review", *Cleaner Materials*, v. 4, pp. 100085, 2022.

[19] ALSAIF, A., ALHARBI, Y.R., "Strength, durability and shrinkage behaviours of steel fiber reinforced rubberized concrete", *Construction & Building Materials*, v. 345, pp. 128295, 2022. doi: http://doi.org/10.1016/j.conbuildmat.2022.128295.

[20] BU, C., ZHU, D., LU, X., *et al.*, "Modification of rubberized concrete: a review", *Buildings*, v. 12, n. 7, pp. 999, 2022. doi: http://doi.org/10.3390/buildings12070999.

[21] BESKOPYLNY, A.N., SHCHERBAN', E.M., STEL'MAKH, S.A., *et al.*, "Composition component influence on concrete properties with the additive of rubber tree seed shells", *Applied Sciences (Basel, Switzerland)*, v. 12, n. 22, pp. 11744, 2022. doi: http://doi.org/10.3390/app122211744.

[22] TOGHROLI, A., MEHRABI, P., SHARIATI, M., *et al*., "Evaluating the use of recycled concrete aggregate and pozzolanic additives in fiber-reinforced pervious concrete with industrial and recycled fibers", *Construction & Building Materials*, v. 252, n. 118997, pp. 118997, 2020. doi: http://doi.org/10.1016/j.conbuildmat.2020.118997.

[23] MEHRABI, P., SHARIATI, M., KABIRIFAR, K., *et al* ., "Effect of pumice powder and nano-clay on the strength and permeability of fiber-reinforced pervious concrete incorporating recycled concrete aggregate", *Construction & Building Materials*, v. 287, n. 122652, 2021.

[24] VENUGOPAL, R., MUTHUSAMY, N., NATARAJAN, B., *et al*., "Statistical optimization of fibre reinforced polymer concrete made with recycled plastic aggregates by central composite design", *Matéria (Rio de Janeiro)*, v. 28, n. 3, pp. e20230182, 2023. doi: http://doi.org/10.1590/1517-7076-rmat-2023-0182.

[25] ZEYBEK, Ö., ÖZKILIÇ, Y.O., ÇELIK, A.İ., *et al*., "Performance evaluation of fiber-reinforced concrete produced with steel fibers extracted from waste tire", *Frontiers in Materials*, v. 9, pp. 1057128, 2022. doi: http://doi.org/10.3389/fmats.2022.1057128.

[26] ZHANG, J., WU, Z., YU, H., *et al*., "Mesoscopic modeling approach and application for steel fiber reinforced concrete under dynamic loading: a review", *Engineering (Beijing)*, v. 16, pp. 220–238, 2022. doi: http://doi.org/10.1016/j.eng.2022.01.011.

[27] AKHTAR, T., ALI, B., KAHLA, N.B., *et al*., "Experimental investigation of eco-friendly high strength fiber-reinforced concrete developed with combined incorporation of tyre-steel fiber and fly ash", *Construction & Building Materials*, v. 314, n. Pt A, pp. 125626, 2022. doi: http://doi.org/10.1016/j.conbuildmat.2021.125626.

[28] ÇELIK, A.İ., ÖZKILIÇ, Y.O., ZEYBEK, Ö., *et al*., "Performance assessment of fiber-reinforced concrete produced with waste lathe fibers", *Sustainability (Basel)*, v. 14, n. 19, pp. 11817, 2022. doi: http://doi.org/10.3390/su141911817.

[29] KHAYAT, K.H., YAHIA, A., SAYED, M., "Effect of supplementary cementitious materials on rheological properties, bleeding, and strength of structural grout", *ACI Materials Journal*, v. 105, n. 6, pp. 585, 2008.

[30] HWANG, K., NOGUCHI, T., TOMOSAWA, F., "Prediction model of compressive strength development of fly-ash concrete", *Cement and Concrete Research*, v. 34, n. 12, pp. 2269–2276, 2004. doi: http://doi.org/10.1016/j.cemconres.2004.04.009.

[31] HOSSAIN, K.M.A., "Volcanic ash and pumice as cement additives: pozzolanic, alkali-silica reaction and autoclave expansion characteristics", *Cement and Concrete Research*, v. 35, n. 6, pp. 1141–1144, 2005. doi: http://doi.org/10.1016/j.cemconres.2004.09.025.

[32] HOSSAIN, K.M.A., "Performance of volcanic ash and pumice-based blended cements in sulphate and sulphate–chloride environments", *Advances in Cement Research*, v. 18, n. 2, pp. 71–82, 2006. doi: http://doi.org/10.1680/adcr.2006.18.2.71.

[33] AYDIN, A.C., GÜL, R., "Influence of volcanic originated natural materials as additives on the setting time and some mechanical properties of concrete", *Construction & Building Materials*, v. 21, n. 6, pp. 1277–1281, 2007. doi: http://doi.org/10.1016/j.conbuildmat.2006.02.011.

[34] DENG, E.F., ZHANG, Z., ZHANG, C.X., et al., "Experimental study on flexural behavior of UHPC wet joint in prefabricated multi-girder bridge", *Engineering Structures*, v. 275, n. Pt B, pp. 115314, 2023. doi: http://doi.org/10.1016/j.engstruct.2022.115314.

[35] ALEX, A.G., JOSE, P.A., SABERIAN, M., *et al*., "Green pervious concrete containing diatomaceous earth as supplementary cementitous materials for pavement applications", *Materials (Basel)*, v. 16, n. 1, pp. 48, 2022. doi: http://doi.org/10.3390/ma16010048. PubMed PMID: 36614394.

[36] XU, C., "Using genetic algorithms method for the paramount design of reinforced concrete structures", *Structural Engineering and Mechanics, An Int'l Journal*, v. 71, n. 5, pp. 503–513, 2019.

[37] KADHAR, S.A., GOPAL, E., SIVAKUMAR, V., "An experimental study on strength and durability properties of self-compacting and self-curing concrete using light weight aggregates", *Matéria (Rio de Janeiro)*, v. 28, pp. e20230156, 2023. doi: http://doi.org/10.1590/1517-7076-rmat-2023-0156.

[38] POURKHORSHIDI, A.R., NAJIMI, M., PARHIZKAR, T., JAFARPOUR, F., & HILLEMEIER, B. (2010). Applicability of the standard specifications of ASTM C618 for evaluation of natural pozzolans. *Cement and Concrete Composites*, *32*(10), 794–800.

[39] LIU, J., MOHAMMADI, M., ZHAN, Y., *et al*., "Utilizing artificial intelligence to predict the superplasticizer demand of self-consolidating concrete incorporating pumice, slag, and fly ash powders",

Materials (Basel), v. 14, n. 22, pp. 6792, 2021. doi: http://doi.org/10.3390/ma14226792. PubMed PMID: 34832194.

[40] MEHRABI, P., HONARBARI, S., RAFIEI, S., *et al*., "Seismic response prediction of FRC rectangular columns using intelligent fuzzy-based hybrid metaheuristic techniques", *Journal of Ambient Intelligence and Humanized Computing*, v. 12, n. 11, pp. 10105–10123, 2021. doi: http://doi.org/10.1007/s12652-020-02776-4. PubMed PMID: 33425053.

[41] TAHERI, E., MEHRABI, P., RAFIEI, S., *et al*., "Numerical evaluation of the upright columns with partial reinforcement along with the utilisation of neural networks with combining feature-selection method to predict the load and displacement", *Applied Sciences (Basel, Switzerland)*, v. 11, n. 22, pp. 11056, 2021. doi: http://doi.org/10.3390/app112211056.

[42] TAHERI, E., FIROUZIANHAJI, A., USEFI, N., *et al*., "Investigation of a method for strengthening perforated cold-formed steel profiles under compression loads", *Applied Sciences (Basel, Switzerland)*, v. 9, n. 23, pp. 5085, 2019. doi: http://doi.org/10.3390/app9235085.

[43] TAHERI, E., FIROUZIANHAJI, A., MEHRABI, P., *et al*., "Experimental and numerical investigation of a method for strengthening cold-formed steel profiles in bending", *Applied Sciences (Basel, Switzerland)*, v. 10, n. 11, pp. 3855, 2020. doi: http://doi.org/10.3390/app10113855.

[44] SHARIATI, M., MAFIPOUR, M.S., MEHRABI, P., *et al*., "Application of Extreme Learning Machine (ELM) and Genetic Programming (GP) to design steel-concrete composite floor systems at elevated temperatures", *Steel and Composite Structures*, v. 33, n. 3, pp. 319–332, 2019.

[45] SHARIATI, M., TRUNG, N.T., WAKIL, K., *et al*., "Moment-rotation of steel rack connections using extreme learning machine", *Steel and Composite Structures*, v. 31, n. 5, pp. 427–435, 2019. doi: http://doi.org/10.12989/SCS.2019.31.5.427.

[46] SHARIATI, M., MAFIPOUR, M.S., MEHRABI, P., *et al*., "Application of a hybrid artificial neural network-particle swarm optimization (ANN-PSO) model in behavior prediction of channel shear connectors embedded in normal and high-strength concrete", *Applied Sciences (Basel, Switzerland)*, v. 9, n. 24, pp. 5534, 2019. doi: http://doi.org/10.3390/app9245534.

[47] SHARIATI, M., TAHMASBI, F., MEHRABI, P., *et al*., "Monotonic behavior of C and L shaped angle shear connectors within steel-concrete composite beams: an experimental investigation", *Steel and Composite Structures*, v. 35, n. 2, pp. 237–247, 2020.

[48] ZHANG, Z., LIANG, G., NIU, Q., *et al*., "A Wiener degradation process with drift-based approach of determining target reliability index of concrete structures", *Quality and Reliability Engineering International*, v. 38, n. 7, pp. 3710–3725, 2022. doi: http://doi.org/10.1002/qre.3168.

[49] HUANG, H., LI, M., YUAN, Y., *et al*., "Theoretical analysis on the lateral drift of precast concrete frame with replaceable artificial controllable plastic hinges", *Journal of Building Engineering*, v. 62, pp. 105386, 2022. doi: http://doi.org/10.1016/j.jobe.2022.105386.

[50] HOSSAIN, K.M., LACHEMI, M., "Development of volcanic ash concrete: strength, durability, and microstructural investigations", *ACI Materials Journal*, v. 103, n. 1, pp. 11, 2006.

[51] BHEEL, N., KEERIO, M.A., KUMAR, A., *et al*., " An investigation on fresh and hardened properties of concrete blended with rice husk ash as cementitious ingredient and coal bottom ash as sand replacement material", *Silicon*,v. 14, n. 8, pp. 1–12, 2021. doi: http://doi.org/10.1007/s12633-020-00906-3.

[52] BHEEL, N., MEMON, F.A., MEGHWAR, S.L., "Study of fresh and hardened properties of concrete using cement with modified blend of millet husk ash as secondary cementitious material", *Silicon*, v. 13, n. 12, pp. 4641–4652, 2021. doi: http://doi.org/10.1007/s12633-020-00794-7.

[53] ALEX, A.G., BASKAR, R., "Behaviour of micro & nano particles in M-sand cement mortar", *International Journal of Applied Engineering Research: IJAER*, v. 11, n. 1, pp. 385–391, 2016.

[54] DONG, Z., QUAN, W., MA, X., *et al*., "Asymptotic homogenization of effective thermal-elastic properties of concrete considering its three-dimensional mesostructure", *Computers & Structures*, v. 279, pp. 106970, 2023. doi: http://doi.org/10.1016/j.compstruc.2022.106970.

[55] HAN, S., ZHENG, D., MEHDIZADEH, B., *et al*., "Sustainable design of self-consolidating green concrete with partial replacements for cement through neural-network and fuzzy technique", *Sustainability (Basel)*, v. 15, n. 6, pp. 4752, 2023. doi: http://doi.org/10.3390/su15064752.

[56] KARRI, S.K., RAO, G.R., RAJU, P.M., "Strength and durability studies on GGBS concrete", *SSRG International Journal of Civil Engineering (SSRG-IJCE)*, v. 2, n. 10, pp. 34–41, 2015.

[57] RAMAN, J.M., KRISHNAN, V., "Partial replacement of cement with GGBS in self compacting concrete for sustainable construction", *International Journal of Civil Engineering*, v. 4, n. 3, pp. 24–28, 2017. doi: http://doi.org/10.14445/23488352/IJCE-V4I3P106.

[58] HOSSAIN, K.M.A., "Blended cement using volcanic ash and pumice", *Cement and Concrete Research*, v. 33, n. 10, pp. 1601–1605, 2003.

[59] ROCHA, P.A.S., URASHIMA, D.C., GUIMARÃES, M.G.A, "Performance of recycled concrete aggregates in the filling of segmental blocks in segmental retaining walls reinforced with geogrids", *Matter (Rio de Janeiro)*, v. 28, pp. e20220251, 2023. doi: https://doi.org/10.1590/1517-7076-RMAT-2022-0251.

[60] LI, W., LUO, Z., TAO, Z., *et al*., "Mechanical behavior of recycled aggregate concrete-filled steel tube stub columns after exposure to elevated temperatures", *Construction & Building Materials*, v. 146, pp. 571–581, 2017. doi: http://doi.org/10.1016/j.conbuildmat.2017.04.118.

[61] HUNG, C.-C., CHANG, J.-N., WANG, H.-Y., *et al*., "Effect of adding waste polyethylene and GGBFS on the engineering properties of cement mortar", *Applied Sciences (Basel, Switzerland)*, v. 12, n. 24, pp. 12665, 2022. doi: http://doi.org/10.3390/app122412665.